ELECTRONIC SUPPLEMENTARY INFORMATION

{111} Faceted $Li_4Ti_5O_{12}$ Octahedra as Reference Electrode Material in Nanostructured Potentiometric CO_2 Sensor

Shravanti Joshi, [a, b, d] *Satyanarayana Lanka,* [d] *Samuel J. Ippolito,* [a, b, c] *Suresh K. Bhargava,* [a, b] *and Manorama V. Sunkara* [b, d]*

[a] Centre for Advanced Materials and Industrial Chemistry (CAMIC), School of Science, College of Science, Engineering & Health Office, RMIT University, Melbourne, VIC 3001, Australia.

[b] RMIT-IICT Research Centre, CSIR-Indian Institute of Chemical Technology, Hyderabad - 500 007, India.

[c] School of Engineering, RMIT University, Melbourne, VIC 3001, Australia.

[d] Nanomaterials Laboratory, Inorganic & Physical Chemistry Division, CSIR-Indian Institute of Chemical Technology, Hyderabad - 500 007, India. E-mail address: manorama@iict.res.in, Tel.: +91 40 27193225; Fax: +91 40 27160921.

* *To whom all Correspondence should be addressed.*

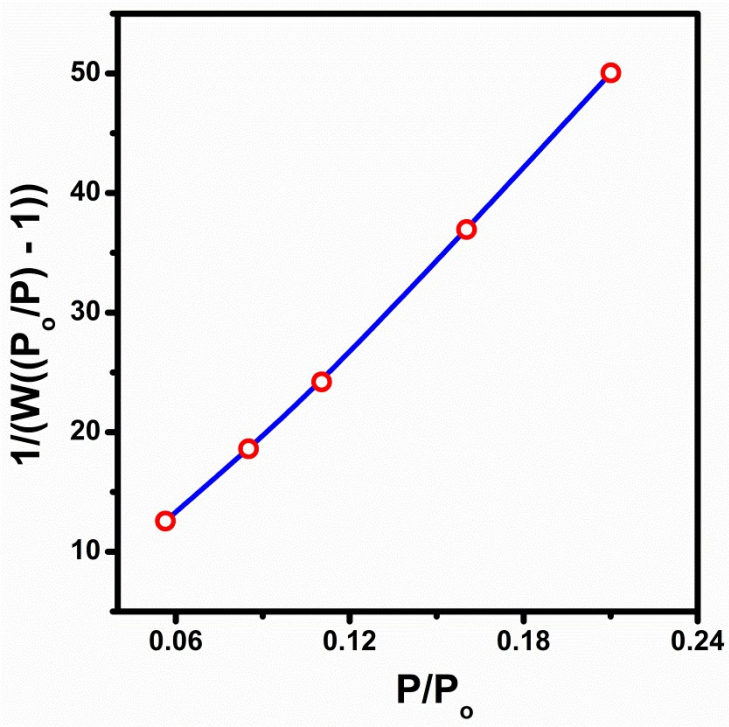

Fig. S1 BET Surface area plot of spinel oxide $Li_4Ti_5O_{12}$ obtained by calcining ternary phase $LiTiO_2$ at 600 ^oC for 2h.

P/P_o	Volume @ STP [cc/g]	$1/ (W((P_o/P)-1))$
5.6472e-02	3.8113	1.256E+01
8.5131e-02	4.0032	1.860E+01
1.1032e-01	4.0995	2.420E+01
1.6031e-01	4.1342	3.695E+01
2.1010e-01	4.2521	5.005E+01

BET Summary

Area = 14.30 m^2/g

Slope = 2.457E+02

Y - Intercept = -2.103E+00

Correlation Coefficient = 0.999055

C = -1.158E+02

Theoretically, we can calculate surface area using BET surface area equation. Using an average range of particle size from FE-SEM and DLS data (50-100nm), an estimate of surface area can be made as below,

$$S\ (BET\ surface\ area) = \frac{6000}{Density\ (\rho) * Particle\ size\ (D_P)}$$

For a particle size of 100 nm and density equal to 3.5 g/cm^3, calculated BET surface area comes around 17 m^2/g which is in close approximation to experimental value (S = 14.30 m^2/g).

Lithium Titanate phase	Route employed	Temperature ^{0}C	Reaction time h	BET surface area m^2/g
Ternary phase ($LiTiO_2$)	Hydrothermal	180	24	20.2
$Li_4Ti_5O_{12}$	Heat Treatment	500	2	18.6
$Li_4Ti_5O_{12}$	Heat Treatment	600	2	14.3
$Li_4Ti_5O_{12}$	Heat Treatment	700	2	12.1

Table 1 BET surface area of as synthesized lithium titanate as function of reaction operating temperature.

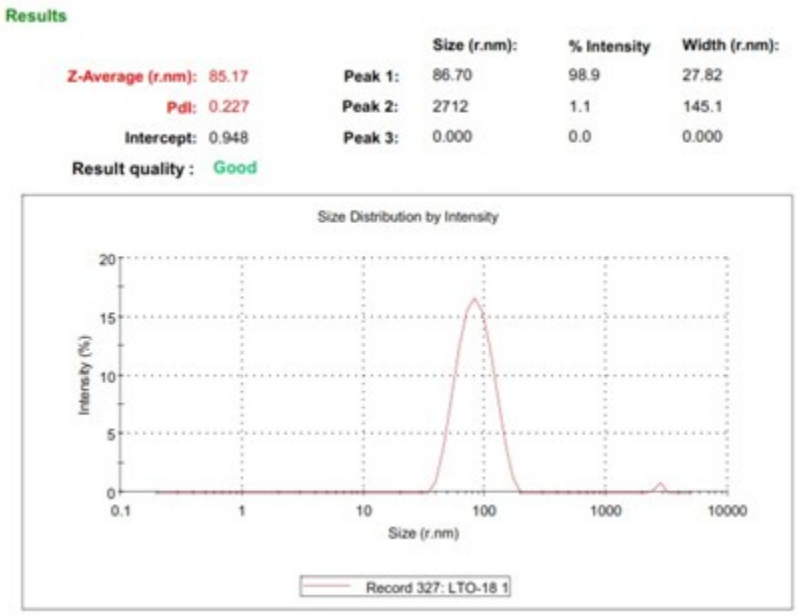

Fig. S2 DLS measurement on intermediate ternary phase $LiTiO_2$ obtained by hydrothermal route at 180 ^oC for 24 h with particles suspended in water.

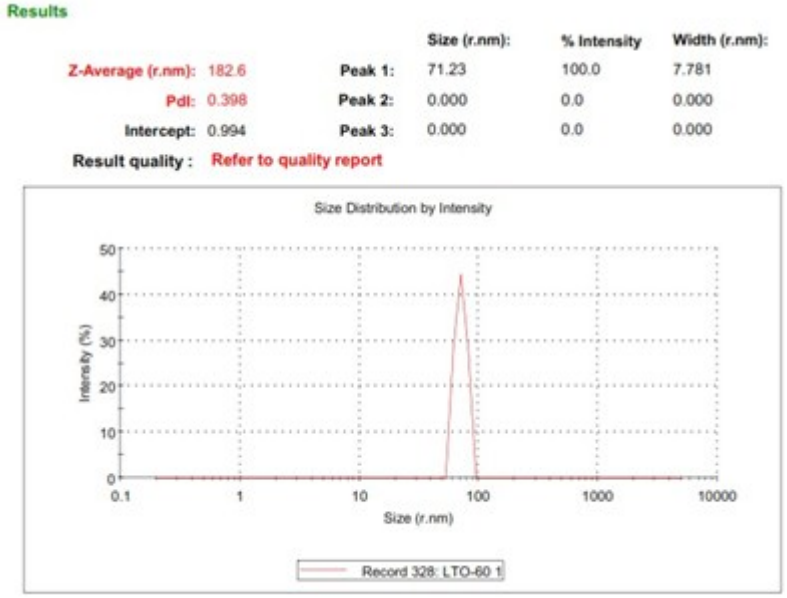

Fig. S3 DLS measurement on spinel oxide $Li_4Ti_5O_{12}$ obtained by calcining the ternary phase $LiTiO_2$ at 600 ^oC for 2 h with particles suspended in water.

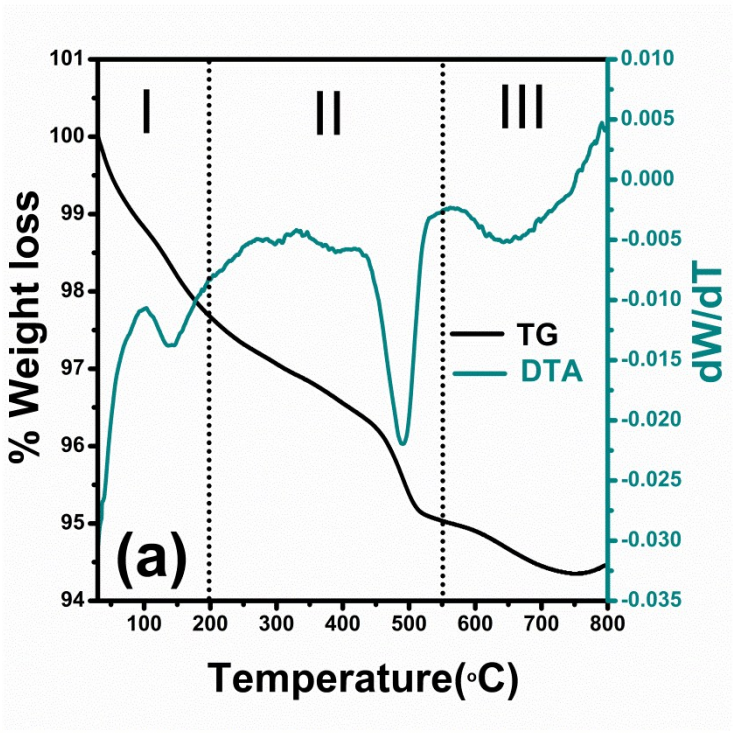

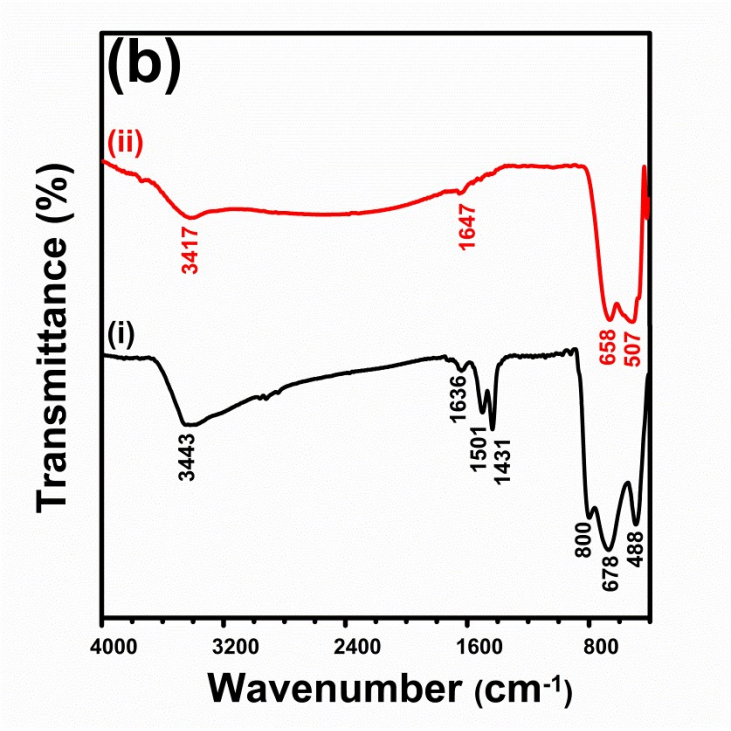

Fig. S4 **(a)** TG-DTA trace of intermediate $LiTiO_2$ phase, **(b)** *mid*-FTIR spectra where **(i)** ternary Li-Ti-O phase obtained by hydrothermal treatment of TiO_2 at 180 °C for 24 h in LiOH solution and **(ii)** spinel $Li_4Ti_5O_{12}$ synthesized by calcining the Li-Ti-O phase at 600 °C for 2 h.

Optimum temperature essential for the formation of chemically phase pure lithium titanium oxide compound was deduced from the thermal decomposition and phase evolution behavior (Fig. **S4.a**) of the oven dried powder studied by TG-DTA in flowing air. The thermal stability of the nanomaterial was assessed by a TA Q50 thermo-gravimetric analyzer. Thermogravimetric scans were recorded at a ramp rate of 10^{o}C/min under nitrogen atmosphere for 10-20 mg samples in the temperature range 35-800 ^{o}C. Analysis of the thermogram was carried out using universal analysis software provided by TA instruments. The intermediate Li-Ti-O ternary phase exhibited weight loss in three main stages. The weight loss of about 4.5% accompanied by an endothermic peak at 140 ^{o}C in the temperature range from 30-200 ^{o}C could be attributed to removal of surface absorbed water.[1,2] Further, a weight loss of 1.65% adjuncted by a sharp endothermic peak at 488 ^{o}C would be associated with decomposition of metal-hydroxide-CTA^{+} complex.[3] The third stage, above 550 ^{o}C corresponding to a weight loss of ~0.5% represents evaporation of volatiles accompanying decomposition of partially formed phase.[4] Here it is assumed that the surfactant degradation takes place in two steps. The first step (350-450 ^{o}C) where surfactant starts to degrade after dehydration of water and which is incompletely accomplished. In the second step (450-550 ^{o}C) remnant surfactant decomposes and the degradation process is completed.[3-4]

Fourier transform infrared spectroscopy (FT-IR) was used to follow the formation of the nanomaterials in the mid absorption range of 4000-400 cm^{-1} employing a Bruker ALPHA-T instrument. Typically, nanomaterial samples (~1 mg) were ground with KBr (~100 mg) and pressed into transparent pellets of approximate dimensions, D=1.2 cm and t=0.02 cm; followed by vacuum drying at 60 ^{o}C for 30 minutes prior to each run. The transmittance spectra collected for 256 scans with a resolution interval 2 cm^{-1}, were corrected for baseline, atmospheric interference and also normalized before comparative evaluation. Fig. **S4.b** shows the *mid*-FTIR

spectrum of $LiTiO_2$ and $Li_4Ti_5O_{12}$ nano octahedra. The broad frequency bands at 3443 and 3417 cm^{-1} can be attributed to stretching vibrations of OH-group originating from Ti-OH.[5] The bands at 1636 and 1647 cm^{-1} are associated with C=O stretching vibrations.[6] Bands at 1501 and 1431 cm^{-1} can be attributed to $-CH_3$ monomer stretching vibrations, and the frequency at 800 cm^{-1} is due to - $(-CH_3)_3$- vibration.[7] Wide band frequencies below 800 cm^{-1} that is, 678, 658, 507 and 488 cm^{-1} are associated with the vibrations of metal organic groups such as Li-O-R or Ti-O-Ti and TiO_6 octahedra stretching.[6-8] Interestingly, it was further observed, that bands at 1501, 1431 and 800 cm^{-1} disappeared when the intermediate ternary phase Li-Ti-O was calcined at 600 ^oC for 2h. It is assumed that this disappearance of the peaks is because of decomposition of the related groups in the solid due to increase in temperature and minimal residual organic compounds in the sample after high temperature calcination. As illustrated in Fig. **S4.b**, the results of FTIR spectra of sample before and after heat treatment are in line with the X-ray diffractograms and *micro*-Raman spectra (Fig. **1a** and **1b**).

The X-ray photoelectron spectroscopy (XPS) data were obtained using Thermo K-alpha system with 180° double focussing hemispherical analyser-128-channel detector. The data were obtained with 150W non-monochromatic Al Kα radiation (1486.6 eV). The C 1s peak centered at 284.60 eV (characteristic of C-C, C=C and C-H bonds) and assigned to aliphatic carbon was used as an internal standard to calibrate all binding energies for residual surface charge due to photoemission. The survey spectrum of $Li_4Ti_5O_{12}$ octahedra showed peaks only from Li, Ti and O (Fig. **S5.a**). The deconvolution of O 1s core level XPS spectrum of oxygen (Fig. **S5.b**), represented by a broad asymmetric peak resulted into four peaks centered at 529.47 eV, 530.45 eV, 531.55 eV and 533.38 eV. The peak at 529.44 eV can be assigned to lattice oxygen in the TiO_2 (O-Ti-O) and the one at 530.45 eV is due to oxygen bonded to lithium. The higher energy

peak at 531.98 eV could be attributed to the oxygen species such as O^{2-} or O^{-} ions present on the surface, while the peak at 532.78 eV can be assigned to adsorbed hydroxyl species.

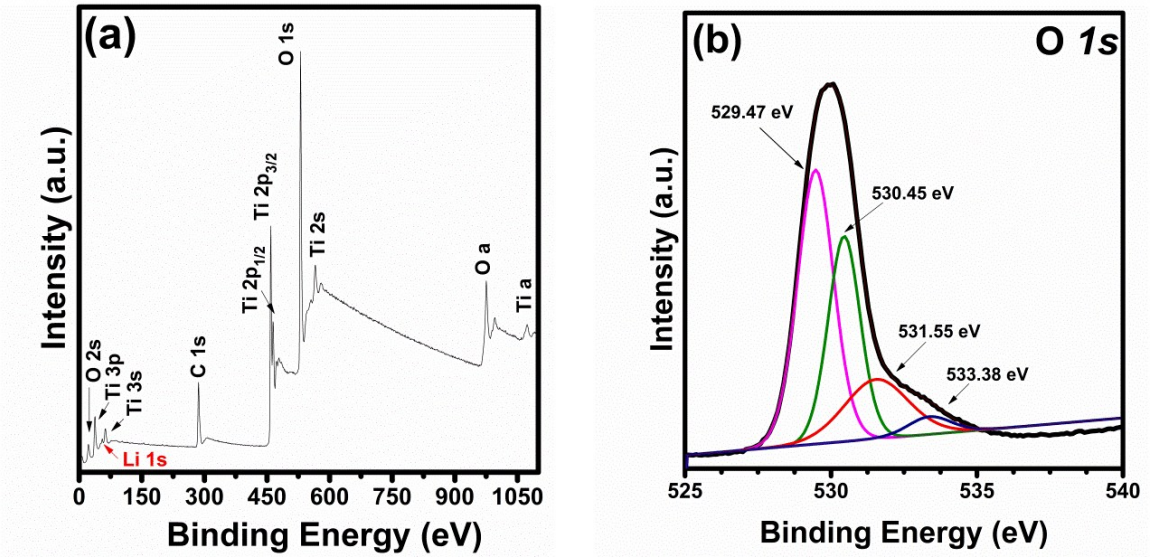

Fig. S5 X-ray photoelectron spectra of spinel $Li_4Ti_5O_{12}$ synthesized by calcining the Li-Ti-O complex at 600 ^{o}C for 2 h where, **(a)** survey spectrum and **(b)** O 1s region.

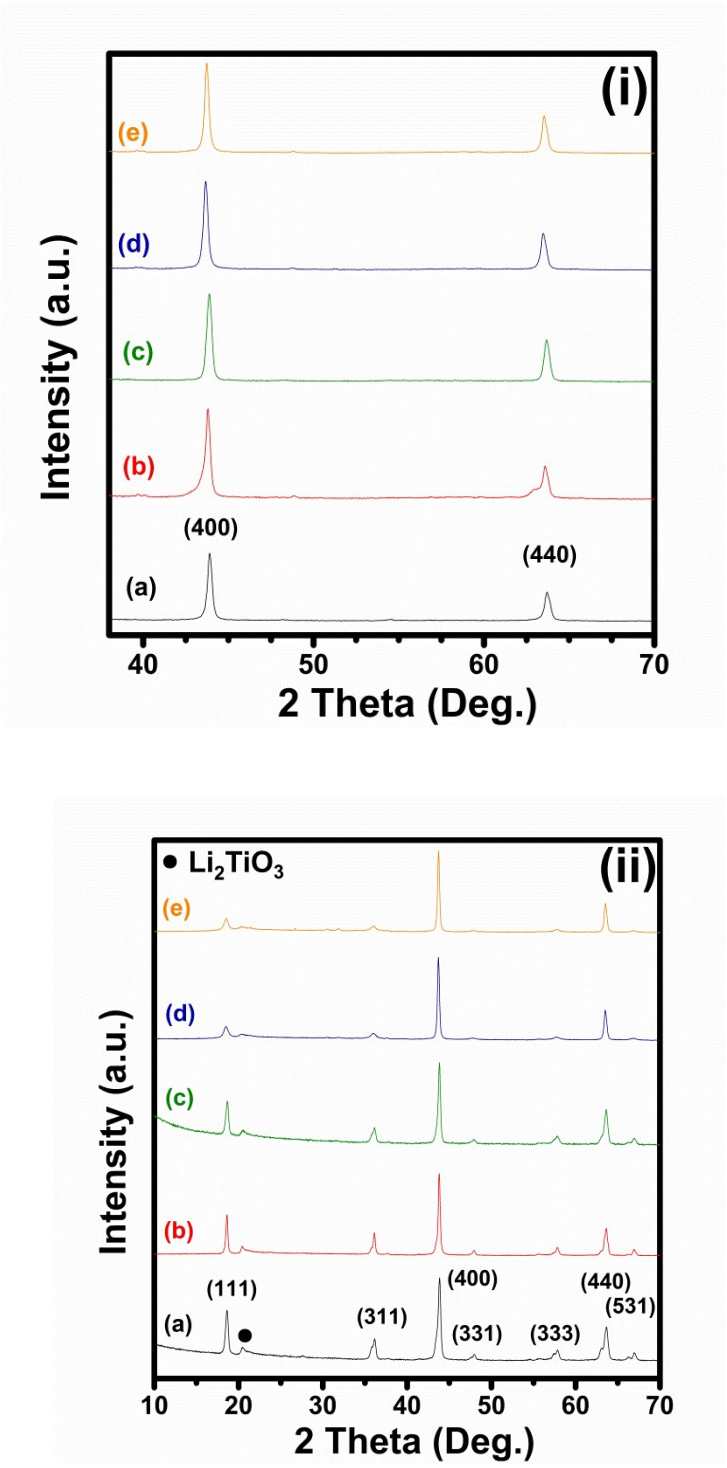

Fig. S6 X-ray diffraction patterns of **(i)** intermediate ternary phase $LiTiO_2$ achieved hydrothermally 180 °C for 24 h, **(ii)** spinel $Li_4Ti_5O_{12}$ as a function of CTAB concentration in mmoles where **(a)** 0, **(b)** 5, **(c)** 10, **(d)** 15 and **(e)** 20.

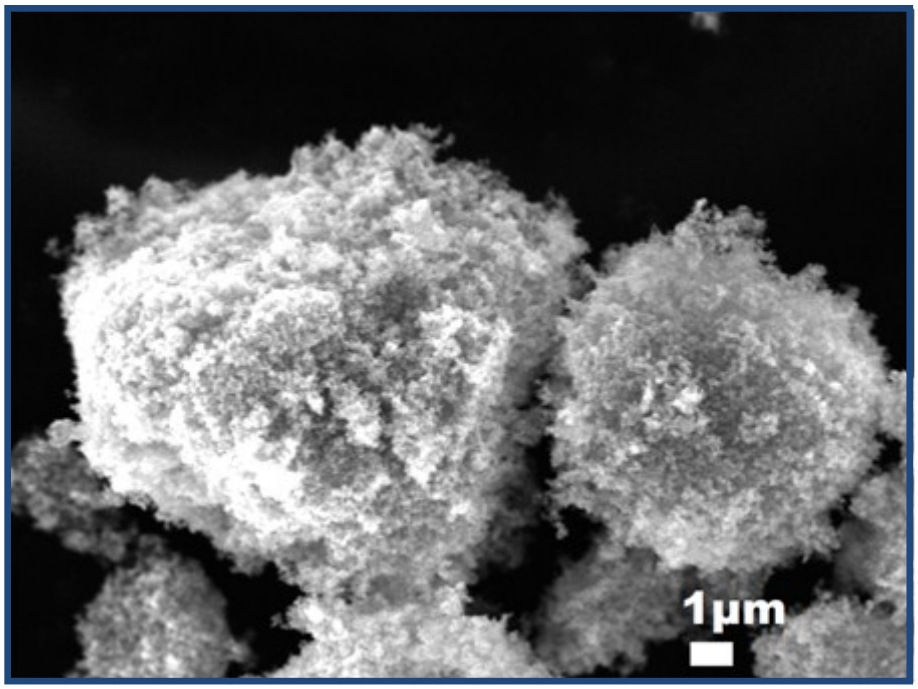

Fig. S7 FE-SEM micrograph of the spinel phase $Li_4Ti_5O_{12}$ without CTAB.

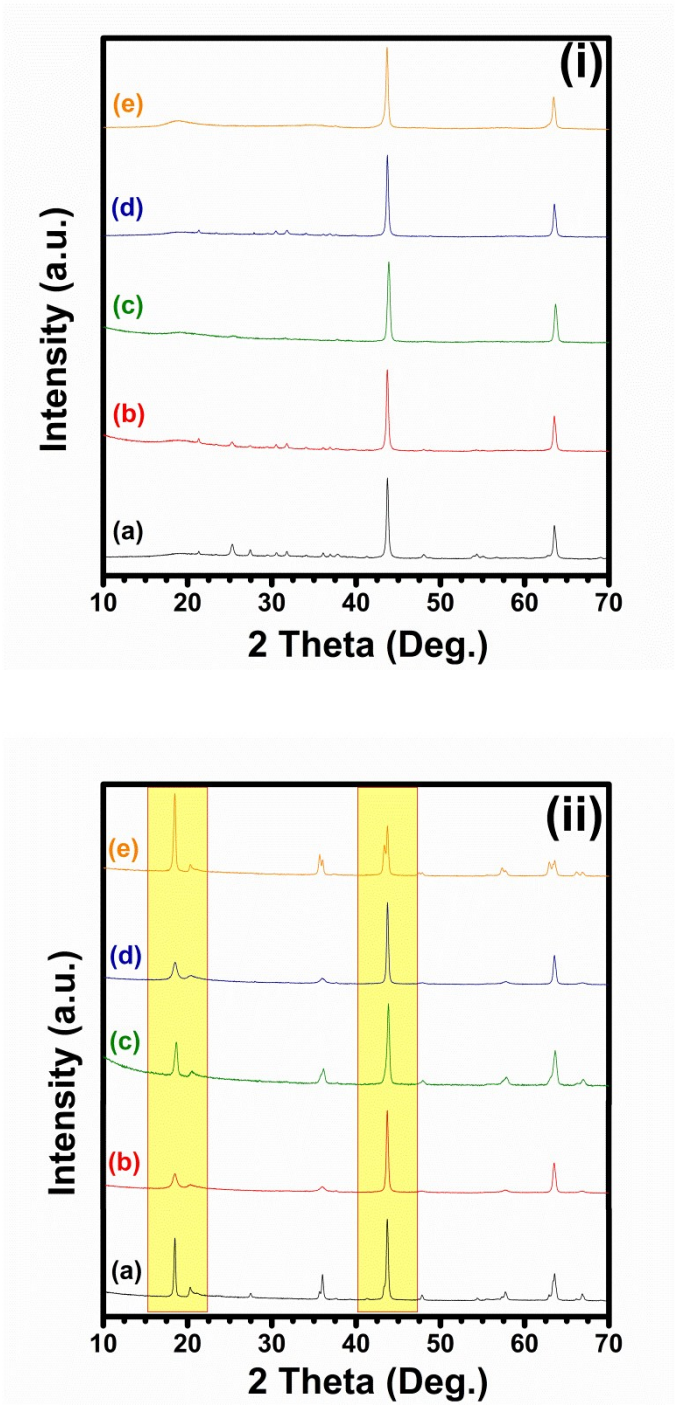

Fig. S8 X-ray diffraction patterns of **(i)** an intermediate ternary phase $LiTiO_2$ at 180 ^oC and **(ii)** spinel $Li_4Ti_5O_{12}$ as a function of hydrothermal reaction time with 10 mmol CTAB concentration **(a)** 6 h, **(b)** 12 h, **(c)** 24 h, **(d)** 36 h and **(e)** 48 h.

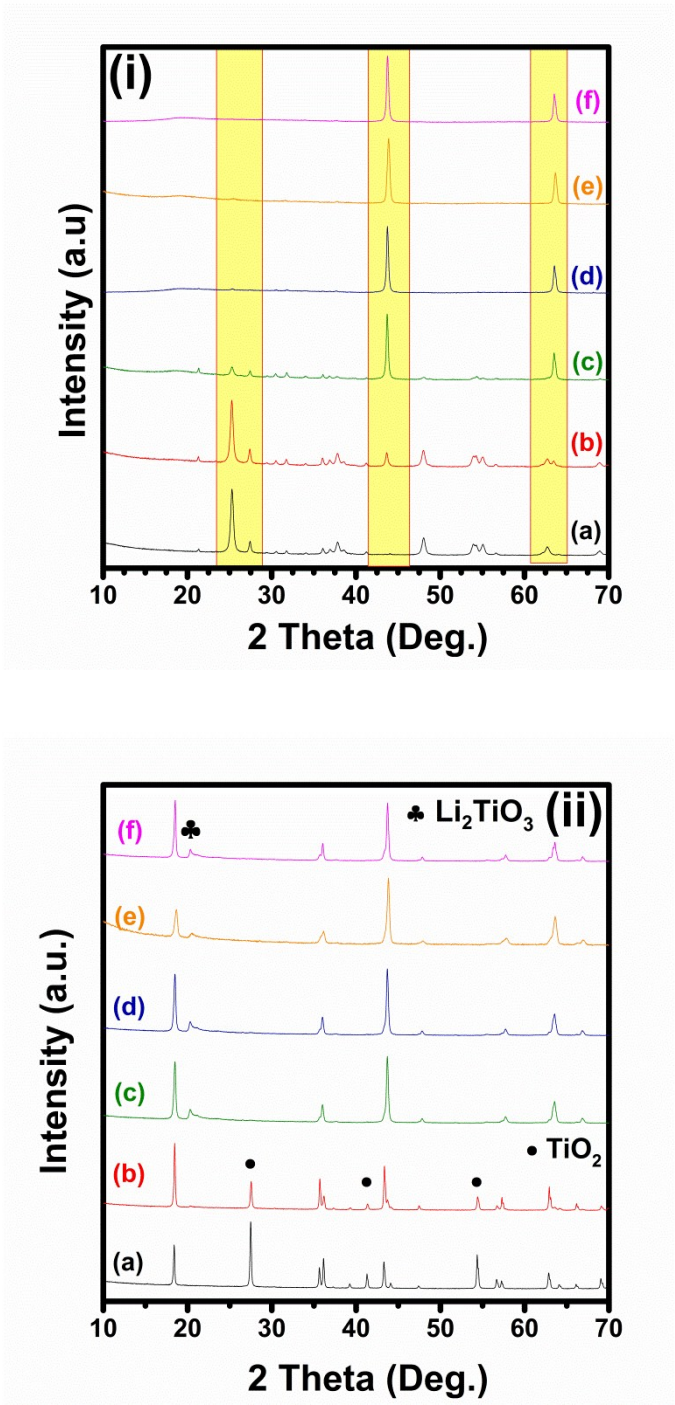

Fig. S9 X-ray diffraction patterns of **(i)** an intermediate ternary phase $LiTiO_2$ and **(ii)** spinel $Li_4Ti_5O_{12}$ as a function of hydrothermal reaction temperature with 10 mmol CTAB concentration and 24 h reaction time **(a)** 100 °C, **(b)** 120 °C, **(c)** 140 °C, **(d)** 160 °C, **(e)** 180 °C and **(f)** 200 °C (*TiO_2 – JCPDS card no: 21-1276, Space group – $P4_2/mnm$ (136)*).

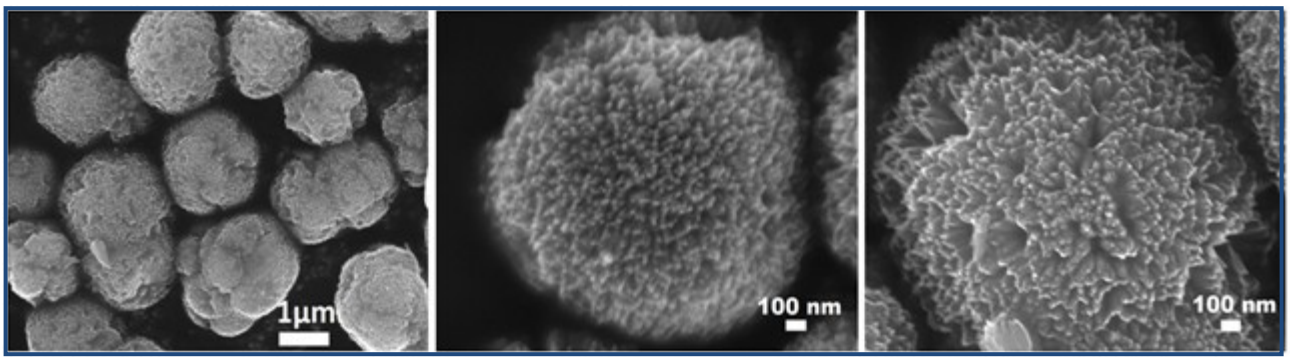

Fig. S10.a Series of electron micrographs depicting 3D TiO_2 hierarchical spheres.

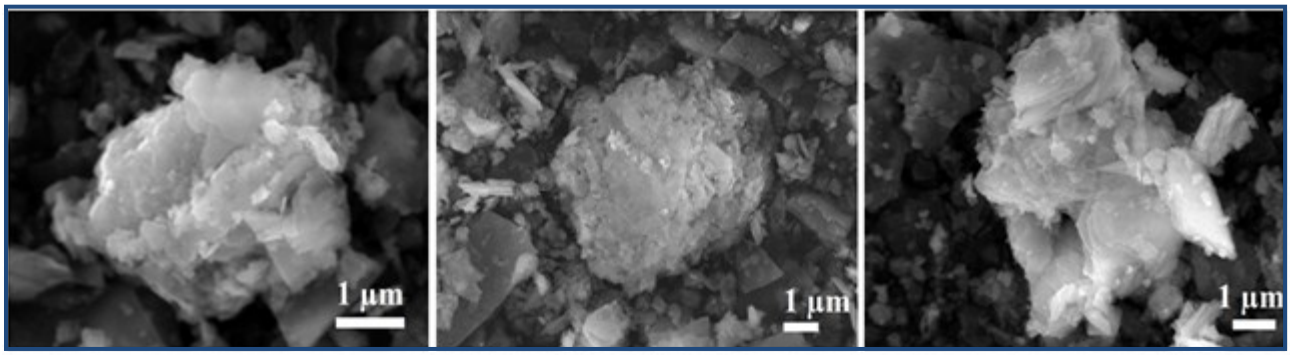

Fig. S10.b Series of electron micrographs depicting 2D Li_2CO_3 flakes.

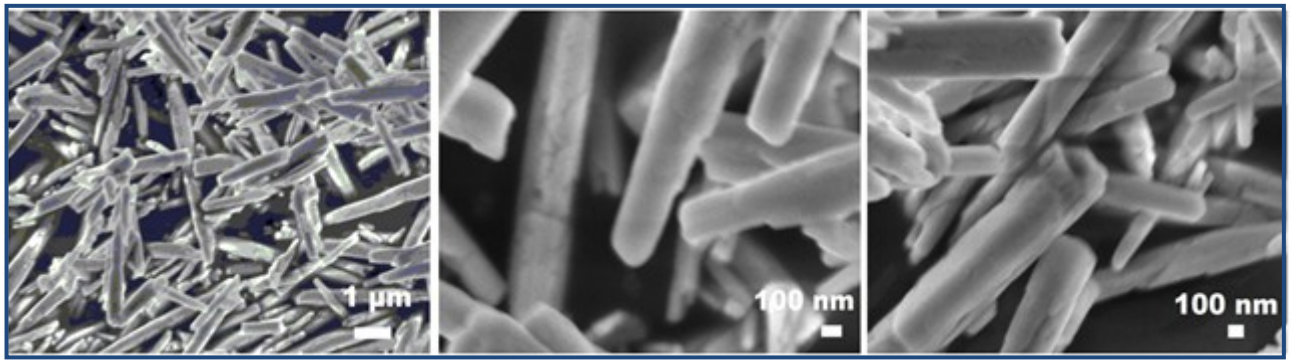

Fig. S10.c Series of electron micrographs depicting 1D $BaCO_3$ rods.

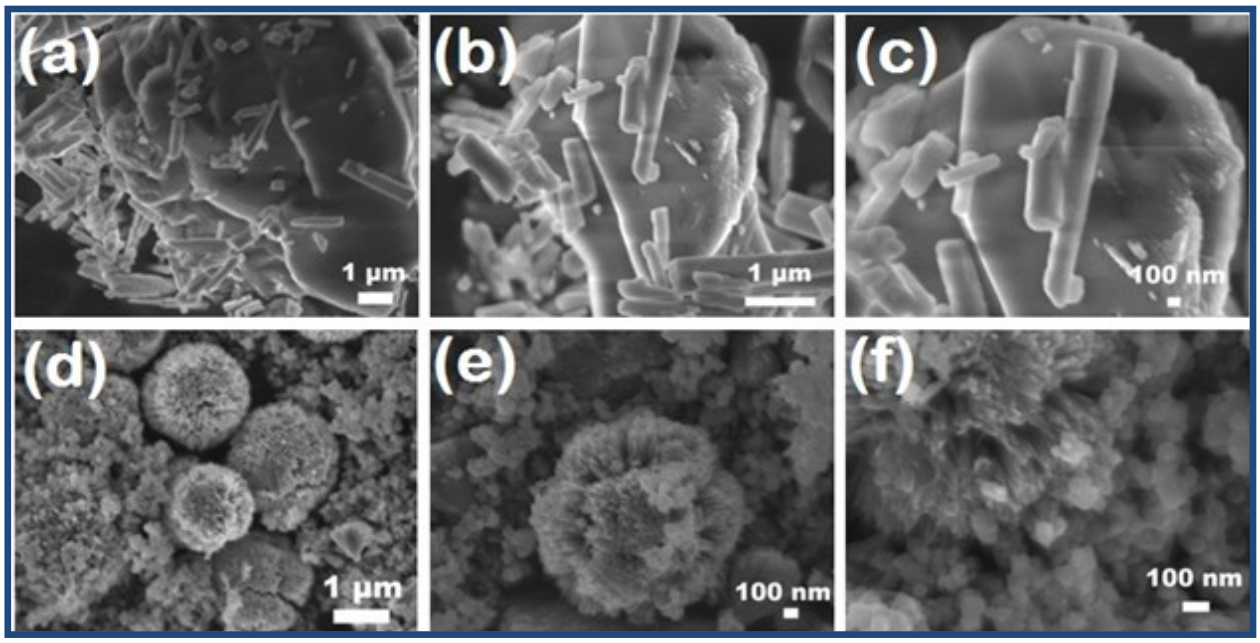

Fig. S10.d FE-SEM micrographs showing hetero-contact formation among sensing and reference electrodes oxide mixtures mixed manually in 90:10 mol %, **(a-c)** 2D $LiCO_3$ flakes with 1D $BaCO_3$ rods and **(d-f)** $Li_4Ti_5O_{12}$ octahedra with TiO_2 rods self assembled in 3D microspheres.

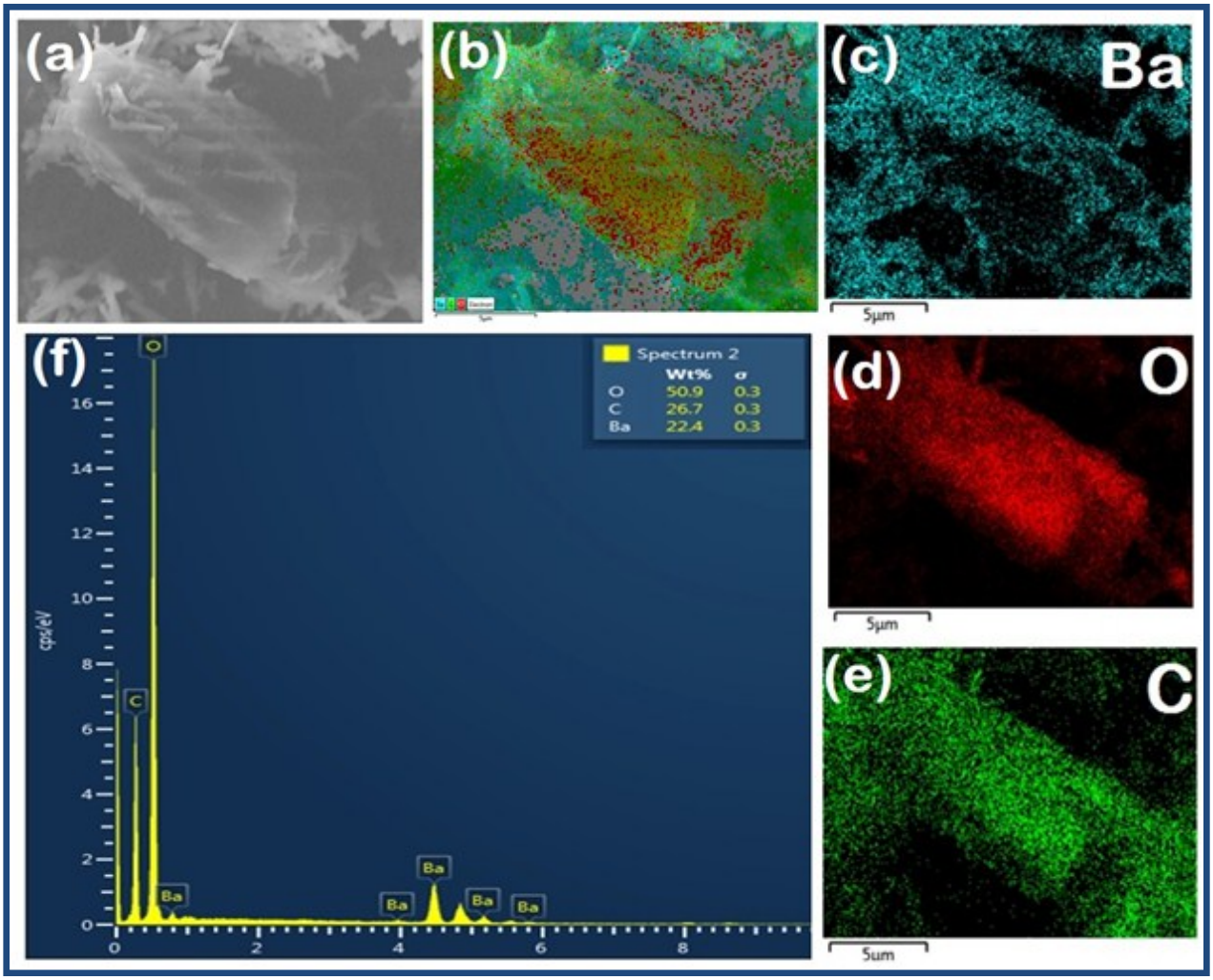

Fig. S11 Clockwise (a) Electron micrograph evincing true area of sensing electrode material that is, Li_2CO_3 mixed manually with $BaCO_3$ in 90:10 mol% ratio used for elemental quantification, **(b)** a layered image, Elemental maps revealing uniform presence of **(c)** barium (Ba), **(d)** oxygen (O), **(e)** carbon (C) throughout the sample, **(f)** EDAX analysis.

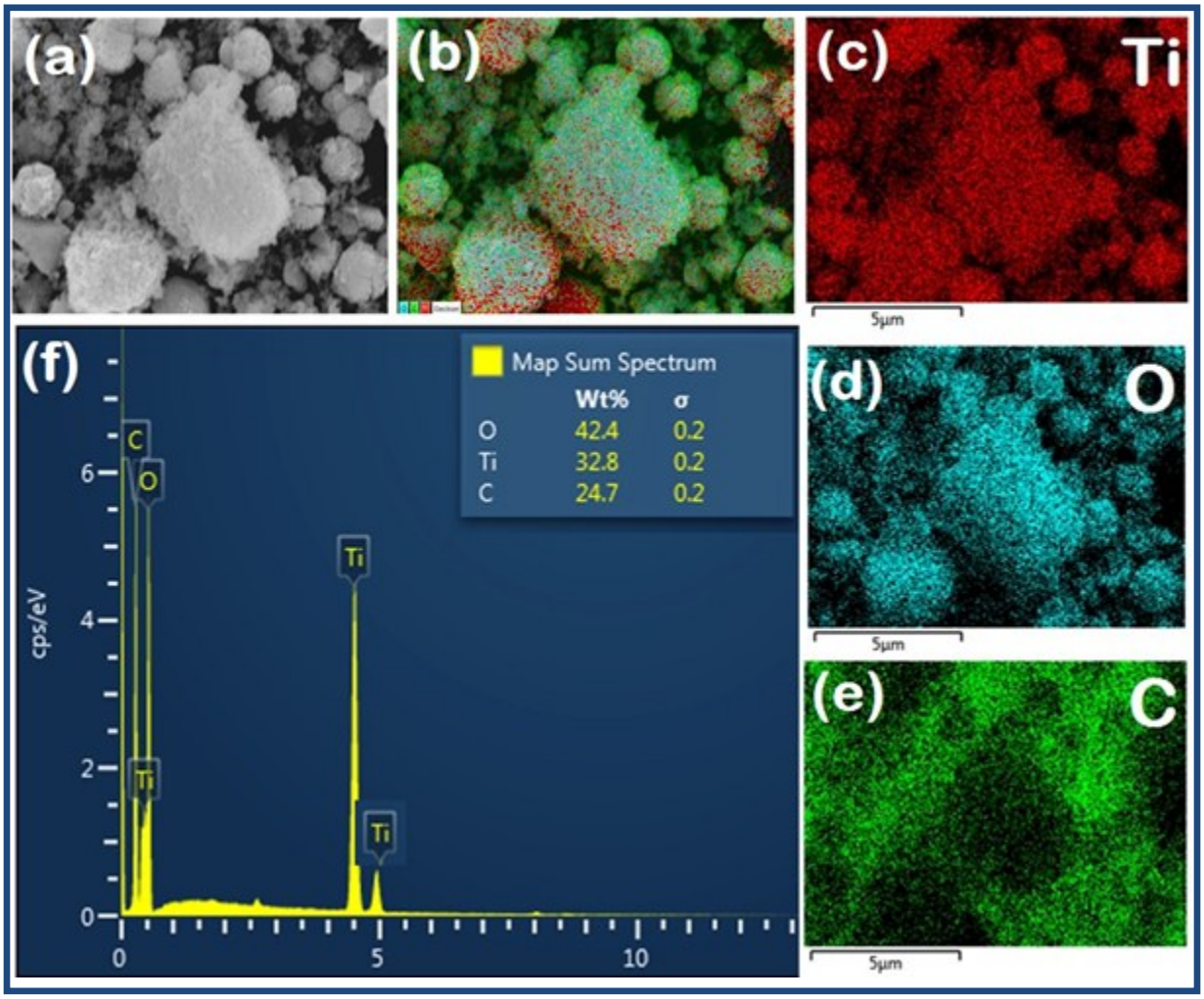

Fig. S12 Clockwise (a) Electron micrograph evincing true area of reference electrode material that is, $Li_4Ti_5O_{12}$ and TiO_2 mixed manually in 90:10 mol% ratio used for elemental quantification, **(b)** Image showing the layers, Elemental maps revealing uniform presence of **(c)** titanium (Ti), **(d)** oxygen (O), **(e)** carbon (C) throughout the sample, **(f)** EDAX analysis. Carbon detected here is due to conductive carbon film used.

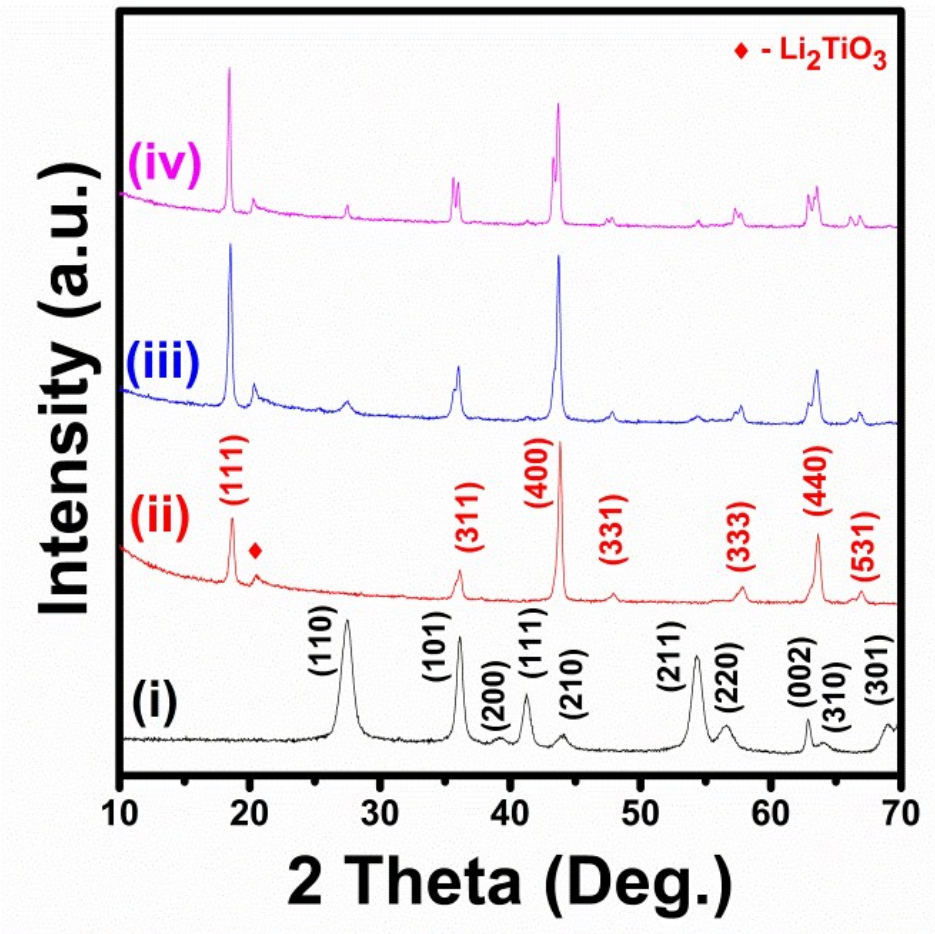

Fig. S13 X-ray diffractograms of reference electrode material where **(i)** Pure TiO_2, **(ii)** $Li_4Ti_5O_{12}$, **(iii)** Oxide mixture of 3D TiO_2 microspheres and $Li_4Ti_5O_{12}$ octahedra in 90:10 mol% ratio mixed physically at room temperature and **(iv)** Oxide mixture sintered at 700 ^oC for 1h.

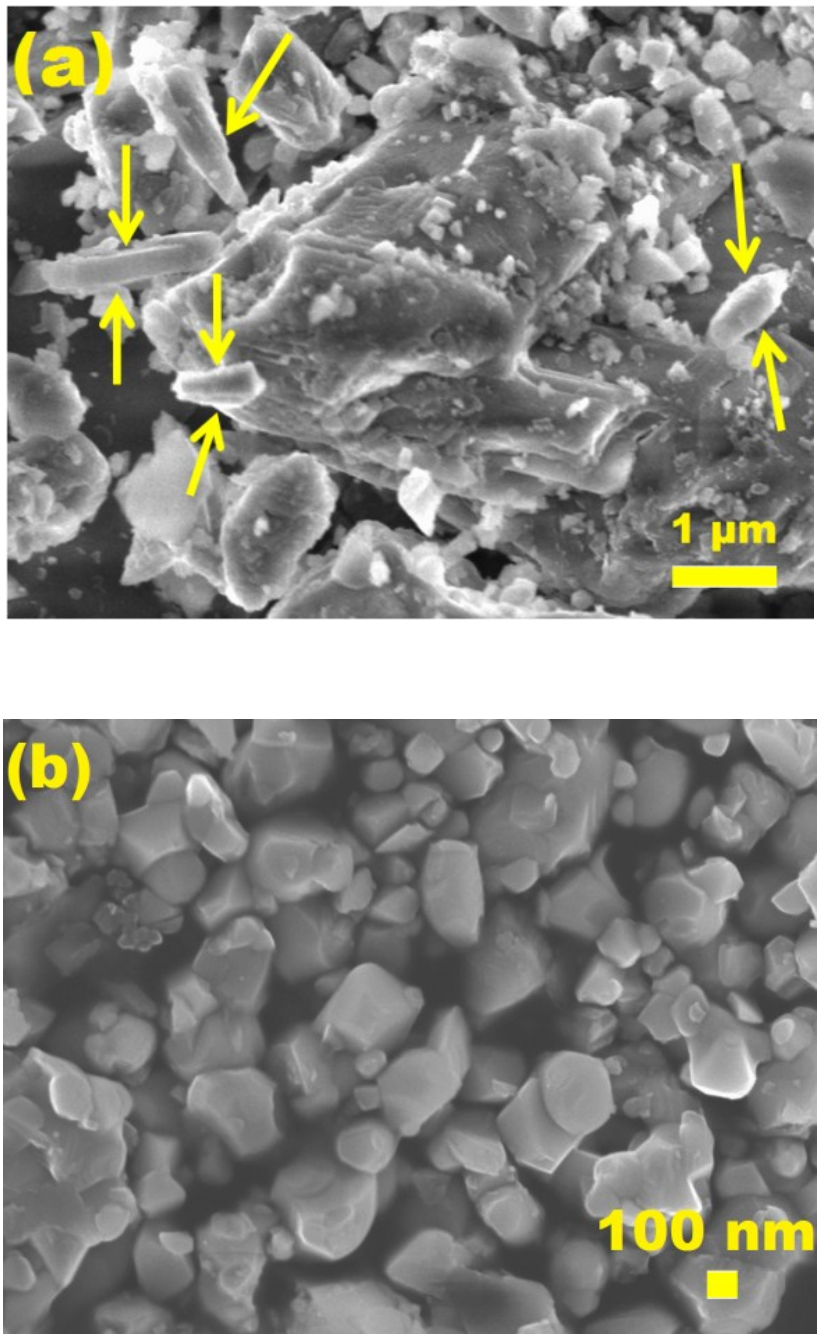

Fig. S14 FE-SEM micrographs showing **(a)** Sensing electrodes oxide mixtures sintered at 600 ^{o}C for 1 h. Here arrows point at 1D $BaCO_3$ rods forming hetero-contact with 2D $LiCO_3$ flakes, **(b)** Reference electrodes oxide mixtures sintered at 700 ^{o}C for 1 h.

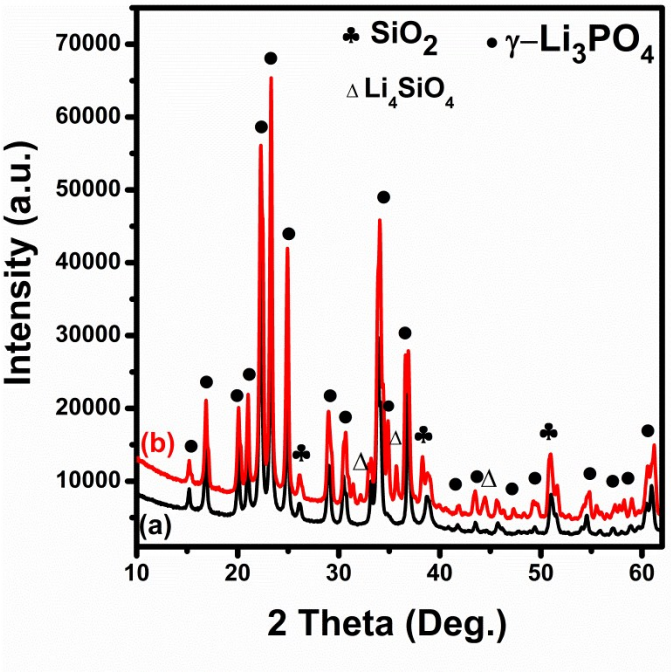

Fig. S15 X-ray diffractograms of Li_3PO_4+SiO_2 (5 mol %) **(a)** before sintering wherein, the commercial Li_3PO_4 and SiO_2 bulk powders were ball milled using distilled water at 300 rpm for 10 h, centrifuged and dried overnight at 80 ^oC, **(b)** after sintering at 800 ^oC for 8 h.

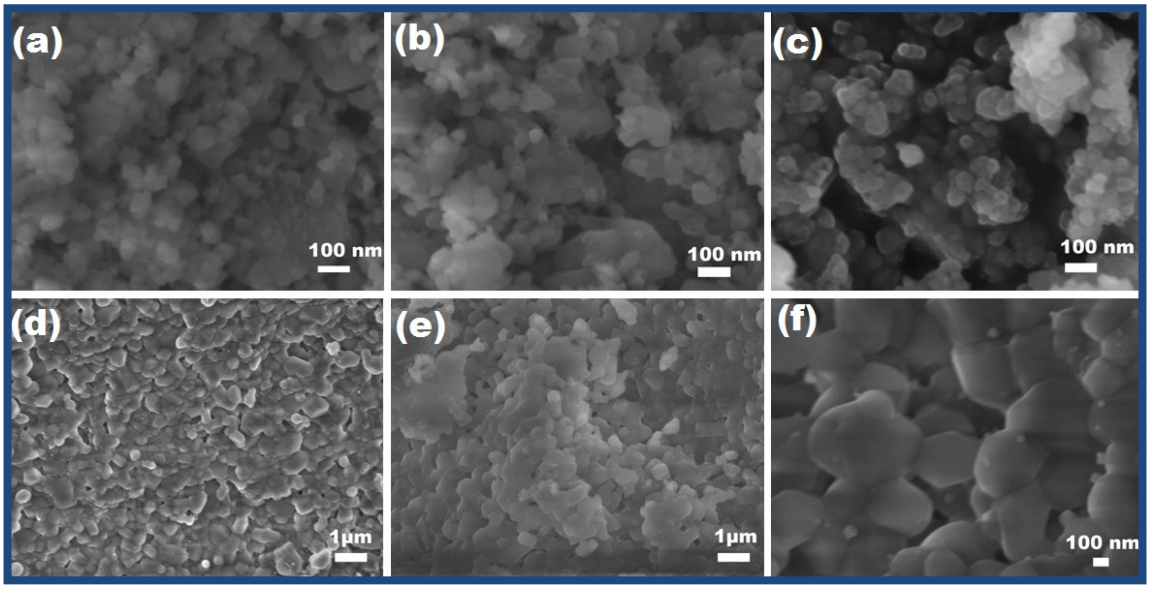

Fig. S16 FE-SEM micrographs of Li_3PO_4+SiO_2 (5 mol %), **(a-c)** before and **(d-f)** after sintering at 800 ^oC for 8 h at a heating and cooling rate of 2 ^oC/min.

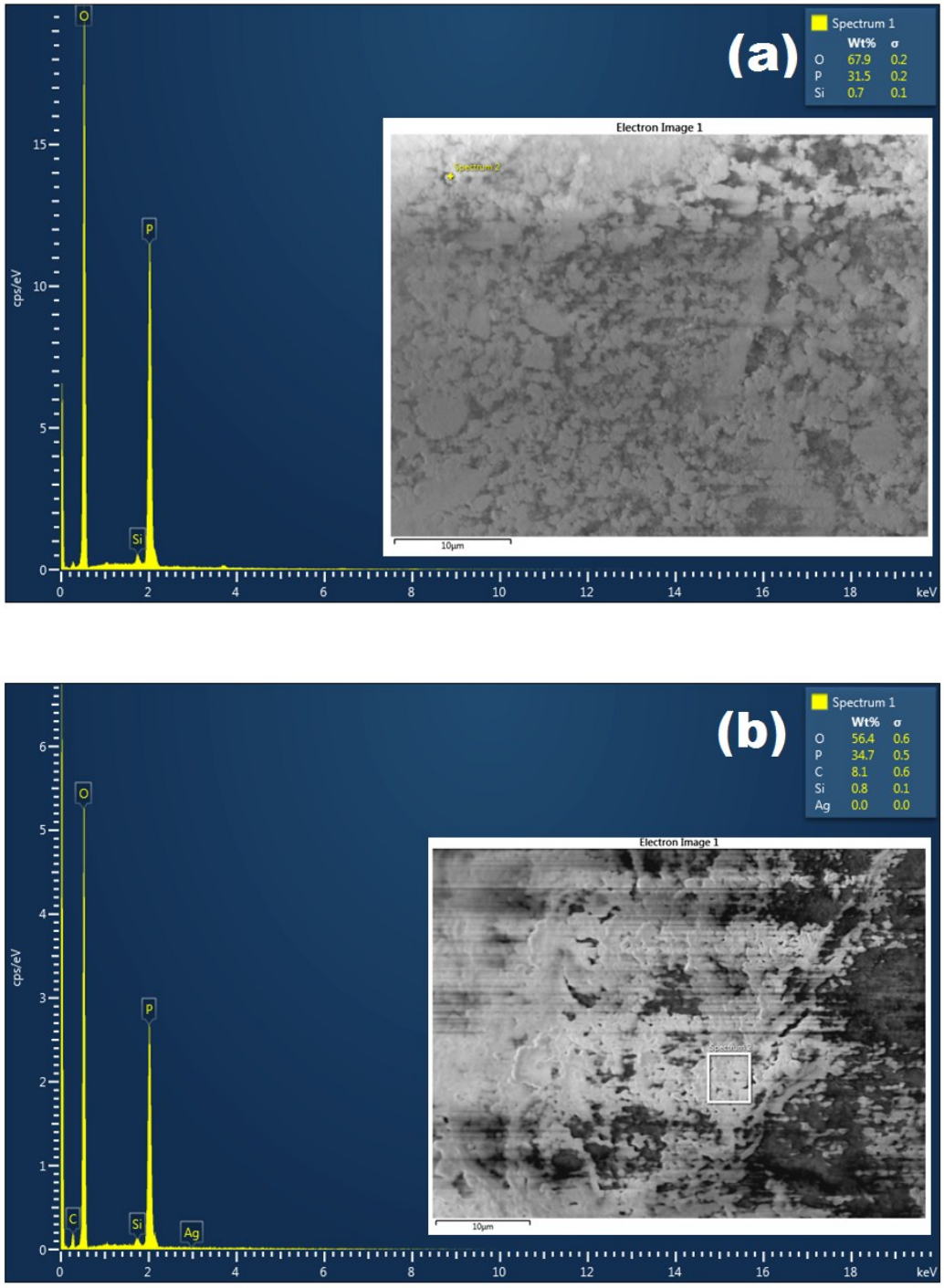

Fig. S17 EDAX analysis of Li_3PO_4+SiO_2 (5 mol %) oxide mixture, **(a)** before and **(b)** after sintering at 800 ^oC for 8 h. **Inset** shows respective electron image with scale 10 µm. Fig **(b)** shows peak due to silver used as electrical contacts.

T (°C)	EMF (mV) 100 ppm	500 ppm	1000 ppm	5000 ppm	10,000 ppm	Nernstian Slope (mV/dec)	n	T.S	E.S
300	-252	-212	-200	-143	-122	65.86	1.72	56.80	52
400	-304	-259	-241	-188	-161	71.17	1.87	66.70	63
500	-384	-336	-310	-254	-233	76.67	1.99	76.60	74
600	-431	-373	-349	-306	-277	74.80	2.31	86.50	82

Table 2 Sensing properties of nanostructured potentiometric CO_2 sensor (NP-sensor) at different operating temperatures as a function of CO_2 gas concentration in dry condition, (Where T.S and E.S are theoretical and experimental sensitivities).

	EMF (mV) 100 ppm	500 ppm	1000 ppm	5000 ppm	10,000 ppm	Nernstian Slope (mV/dec)	n
Dry CO_2	-384	-336	-310	-254	-233	76.67	1.99
Wet CO_2	-384	-331	-305	-249	-229	78.43	1.95

Table 3 Sensing properties of nanostructured potentiometric CO_2 sensor (NP-sensor) at a constant working temperature of 500 °C in dry and wet conditions.

	EMF (mV) 100 ppm	500 ppm	1000 ppm	5000 ppm	10,000 ppm	Nernstian Slope (mV/dec)	n
Dry CO_2	-470	-415	-392	-341	-317	75.98	2.01
Wet CO_2	-470	-415	-387	-336	-312	78.85	1.94

Table 4 Sensing properties of commercial potentiometric CO_2 sensor (CP-sensor) at a constant working temperature of 500 °C in dry and wet conditions.

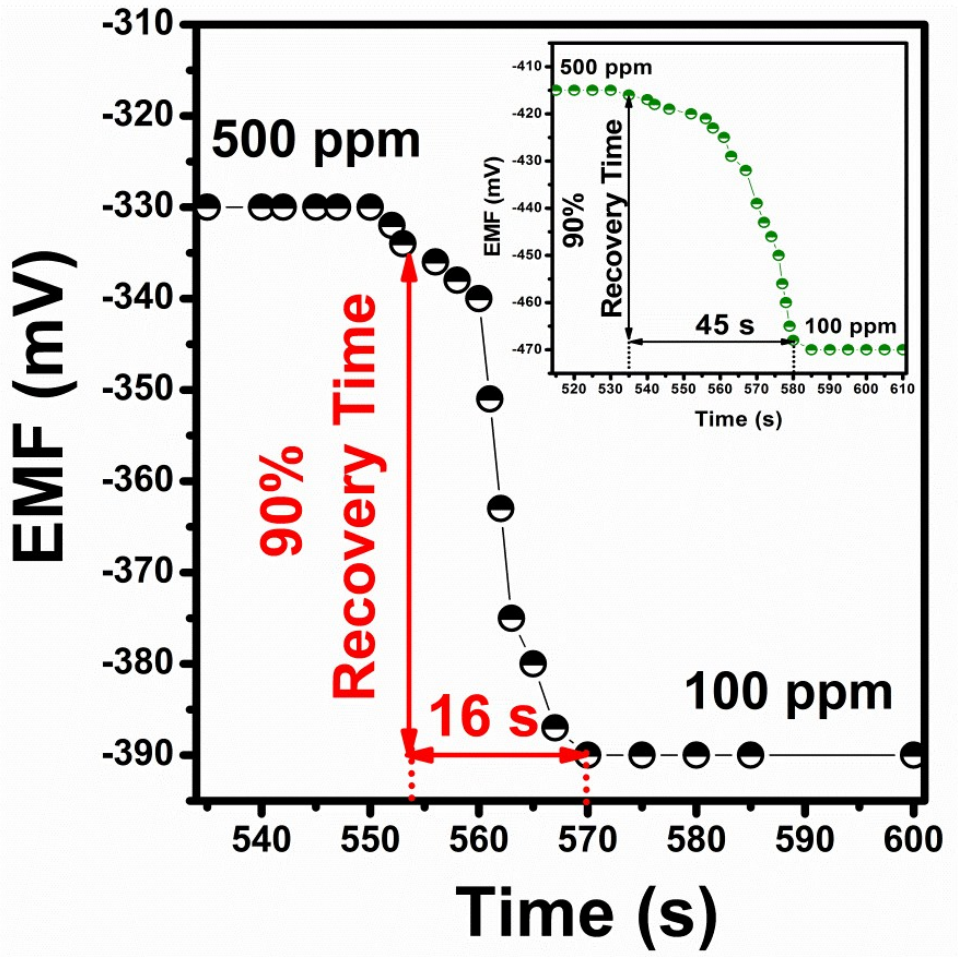

Fig. S18 Recovery characteristics of NP-sensor towards CO_2 gas in dry air (**Inset** shows the recovery time of CP-sensor).

Supplementary References

1 P. Manjula, B. Ramireddy and S.V. Manorama, ACS *Appl. Mater. Inter.,* 2012, **4**, 6252.

2 A. Shanmugasundaram, P. Basak, S. V. Manorama, B. Krishna and S. Srinath, *ACS Appl. Mater. Inter.,* 2015, **7**, 7679.

3 D. Ramimoghadam, M. Z. B. Hussein, Y. H. Taufiq-Yap, *Int. J. Mol. Sci.,* 2012, **13**, 13275.

4 R. Denoyel, M. T. J. Keene, P. L. Llewellyn, J. Rouquerol, *J. Therm. Anal. Calorim,* 1999, 56, 261.

5 D. C. L. Vasconcelos, V. C. Costa, E. H. M. Nunes, A. C. S. Sabioni, M. Gasparon and W. L Vasconcelos, *Materials Sciences and Applications,* 2011, **2**, 1375.

6 C. M. Julien and K. Zaghib, *Electrochim. Acta,* 2004, **50**, 411.

7 Y. Li, H. Zhao, Z. Tian, W. Qiu and X. Li, *J. Alloys Compd.,* 2008, **455**, 471.

8 R. Sui, A. S. Rizkalla and P. A. Charpentier, *J. Phys. Chem. B.,* 2006, **110**, 16212.